SEMARAK ILMU PUBLISHING

Journal of Advanced Research in Numerical Heat Transfer

Journal homepage:
https://semarakilmu.com.my/journals/index.php/arnht/index
ISSN: 2735-0142


# Numerical Simulation to Investigate Interactions of Generated Underwater Micro Shock Waves and Micro Bubbles by Focusing Femtosecond Pulse Laser

Ayumu Yamamoto[1,*], Kazuteru Toh[1], Masaaki Tamagawa[1]

[1] Department of Life Science and Systems Engineering, Graduate School of Life Science and Systems Engineering, Kyushu Institute of Technology, Kitakyushu, Wakamatsu, Fukuoka 808-0196 Japan

**ARTICLE INFO**

***Article history:***
Received 7 March 2023
Received in revised form 13 April 2023
Accepted 15 May 2023
Available online 30 June 2023

***Keywords:***
Regenerative medicine; Cell culture; Femtosecond pulse laser; Laser-induced shock wave; Micro bubble

**ABSTRACT**

The purpose of this study is to elucidate the mechanism of propagation of the laser-induced micro shock waves under condition where the micro bubbles are generated. In this paper, effects of generated micro bubbles on propagation of the laser-induced micro shock waves were investigated by CFD (computational fluid dynamics). Firstly, the two models (1-D model and 1-D spherical symmetric model) were computed for comparison of the peak pressure variation of the shock waves with propagation. As for governing equations for the propagation of the shock waves, continuity equation, Euler's momentum equation and Tait's state equation are used. From the computation, it is confirmed that attenuation of pressure of the 1-D spherical symmetric model was earlier than the 1-D model. In addition, the attenuation of the 1-D spherical symmetric model agreed with the laser-induced shock waves obtained experimentally. However, the peak pressure and duration time of the shock wave was not the same as the experimental result. Then, the bubble behavior was included in the computation of the shock wave propagation. As for the bubble behavior, Rayleigh-Plesset equation is used. From this computation, pressure wave was obtained which superposed the pressure of the shock wave on the internal pressure of the bubble. Although the duration time of the pressure wave was close to the experimental result, the value of the pressure was almost the same as atmospheric pressure. It is suggested that there is a possibility that phenomenon other than the bubbles is generated such as plasma when the shock wave is generated by focusing the femtosecond pulse laser.

## 1. Introduction

Shock wave technologies have been applied to medical field such as extracorporeal shock wave lithotripsy (ESWL) and ossification. Recently, some research has reported that cultured cells, living tissue and vascular endothelial cells have been activated by shock wave stimulation [1-3]. In the field of regenerative medicine, it is needed to cultivate the cell and restore the tissue efficiently and quickly for organ production. Shock wave stimulus can be expected to streamline and shorten the

* *Corresponding author.*
*E-mail address: yamamoto.ayumu226@mail.kyutech.jp (Ayumu Yamamoto)*

https://doi.org/10.37934/arnht.13.1.1830

process. In previous research, the development of a regenerative medical system which combined the acceleration of cell culture and destruction of DDS (drug delivery system) capsule was conducted by applying shock wave technology [4,5]. To selectively stimulate individual capsules and cells, it is necessary to generate micro shock waves with active area of micrometer order. The pulse laser is used to generate micro shock waves [6-10]. When a microsecond or nanosecond pulse laser is focused on water, a shock wave is generated due to the temperature rise and thermal expansion at the laser-focal area. These laser-induced shock waves are not applicable to the cells and the living tissue because the thermal energy is accumulated in a media. On the other hand, a focusing femtosecond pulse laser generates shock waves due to the rapid increase of the energy in the ultra-short duration. Since the energy cannot translate to thermal energy because of the short duration, the thermal effects on media can be suppressed.

In recent papers, femtosecond pulse laser-induced shock waves were used to isolate adherent cells as a manipulator and its effectiveness is verified in the field of biology [11-13]. In addition, micro bubbles have been observed at the laser-focal point when focusing the laser and generating shock waves. From the research of laser dynamics, the theoretical understanding of the generation of the shock waves and the bubbles has been presented [14]. When the femtosecond pulse laser is focused on water, the pressure increases rapidly by multiphoton absorption at the laser focal area. As the pressure relaxes over time, the focal area instantly becomes low pressure and it is considered the nucleus of the bubble is formed. However, the interaction between shock waves and micro bubbles, as well as their characteristics have not been sufficiently investigated. As a physical property, the pressure of the femtosecond pulse laser-induced shock waves and the radius of the micro bubble have been measured in our previous experiments [15,16]. It is difficult to investigate the interaction by only the experiments because the propagation of the shock waves and the behavior of the micro bubbles are fast phenomena in a micro area.

The purpose of this study is to elucidate the mechanism of propagation of the laser-induced micro shock waves under condition where the micro bubbles are generated. In this paper, the effects of the generated micro bubbles on the propagation of the laser-induced micro shock waves were investigated by CFD. Firstly, the peak pressure variation of the shock waves with shock wave propagation is compared between the two shock wave models which do not consider the effects of bubbles. Secondly, the propagation of the shock waves was computed considering the bubble behavior.

## 2. Computational Models and Conditions for Propagating Shock Waves

### *2.1 Computational Assumption of Generation of Shock Waves*

Figure 1 shows a conceptual diagram of the computational model. It is assumed that 100 % of laser energy transfers to the laser-focal area. The shock waves are generated from the laser-focal area. The micro bubble is positioned at the laser-focal area in advance in the case of considering its effects. Here, theoretical diameter of the laser-focal area df is calculated with the following equation [17]:

$$d_{\mathrm{f}} = 1.22\frac{\lambda}{NA} \tag{1}$$

where $\lambda$ is wavelength of the laser and $NA$ is numerical aperture of objective lens. Eq. (1) expresses that the laser-focal energy is mainly determined by the numerical aperture of the objective lens. Here, $\lambda$ was fixed to be 1030 nm and $NA$ was fixed to be 0.5 as per the previous experiments [16,17]. The diameter of the laser-focal area was calculated to be 2.51 μm from Eq. (1).

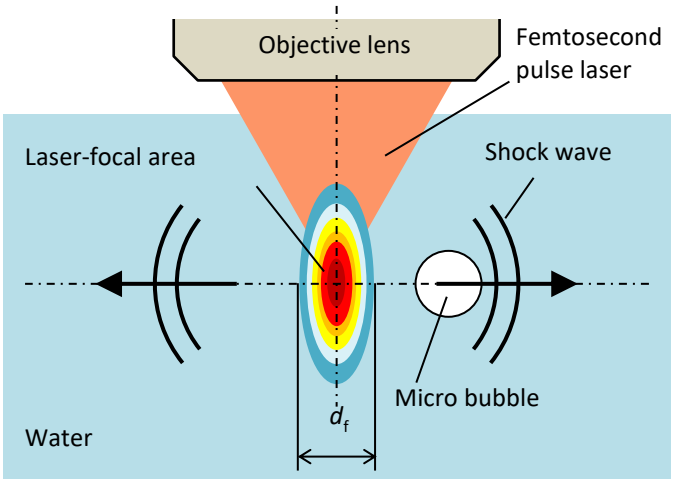


**Fig. 1.** Conceptual diagram of the computational model

### *2.2 Governing Equations for Propagation of Shock Waves in 1-D Model*

In this section, the governing equations for the propagation of the shock waves without the bubble behavior are explained. For comparison of the propagation characteristics, both 1-D model (plane shock wave) and 1-D spherical symmetric model (spherical shock wave) are computed. Firstly, the continuity equation and Euler's momentum equation are used as the governing equations of the 1-D model.

$$\frac{\partial \rho}{\partial t} + \frac{\partial}{\partial x}(\rho v) = 0 \tag{2}$$

$$\frac{\partial}{\partial t}(\rho v) + \frac{\partial}{\partial x}(\rho v^2) + \frac{\partial p}{\partial x} = 0 \tag{3}$$

where $\rho$ is density, $v$ is velocity and $p$ is pressure. As the state equation of water, Tait's state equation is applied to the computation.

$$\left(\frac{p+B}{p_0+B}\right) = \left(\frac{\rho}{\rho_0}\right)^Z \tag{4}$$

where, the parameter $p_0$ is 101.3 kPa, $\rho_0$ is 998.2 kg/m$^3$, $Z$ is 3.14 and $B$ is 304.9 MPa. Due to the conditions of $Z$ and $B$, the pressure is limited to the range of 0 to 100 MPa in this computation.

As a method of discretization, the TVD (total variation diminishing) method was used for the continuity equation and Euler's momentum equation. The TVD method is a variant of the upwind difference method for capturing shock waves [18]. The scheme suppresses numerical oscillations and maintains monotonicity in analyses with discontinuous surfaces such as shock waves. In addition, Hartrn's flux correction method was used in this computation [19].

### *2.3 Governing Equations for Propagation of Shock Waves in 1-D Spherical Symmetric Model*

Generally, the laser-induced shock waves propagate spherically in water. In this computation, the propagation of the spherical shock wave is simulated by the 1-D spherical symmetric model which is computed by the following equations:

$$\frac{\partial \rho}{\partial t} + \frac{1}{r^2}\frac{\partial}{\partial r}(r^2 \rho v) = 0 \tag{5}$$

$$\frac{\partial}{\partial t}(\rho v) + \frac{1}{r^2}\frac{\partial}{\partial r}(r^2 \rho v^2) + \frac{1}{r^2}\frac{\partial}{\partial r}(r^2 p) = 0 \tag{6}$$

where Eq. (5) and Eq. (6) are converted to a conservative system.

$$\frac{\partial}{\partial t}(r^2 \rho) + \frac{\partial}{\partial r}(r^2 \rho v) = 0 \tag{7}$$

$$\frac{\partial}{\partial t}(r^2 \rho v) + \frac{\partial}{\partial r}\{r^2(\rho v^2 + p)\} = 2rp \tag{8}$$

The propagation of 1-D spherical symmetric shock waves is computed by Eq. (7) and Eq. (8). These equations are also discretized by the TVD method.

### *2.4 Computational Model and Boundary Conditions*

Figure 2 shows the computational model. To simulate the generation of the shock wave from the laser-focal area, by setting the initial high-pressure part which is the almost same size as the theoretical radius. The width of the initial high-pressure part is fixed to be 1.32 μm. In reality, as the pressure is determined by Tait's state equation, it is necessary to fix the density as a computational condition. From the previous experiments, the initial high-pressure $p_H$ is fixed to be 6.0 MPa ($\rho_H$ = 1000.88 kg/m$^3$) based on the estimated pressure at the laser-focal area [16]. For the initial low-pressure part which simulated the surrounding liquid, the pressure $p_L$ is fixed to be 0.1 MPa ($\rho_L$ = 998.20 kg/m$^3$) as atmospheric pressure.

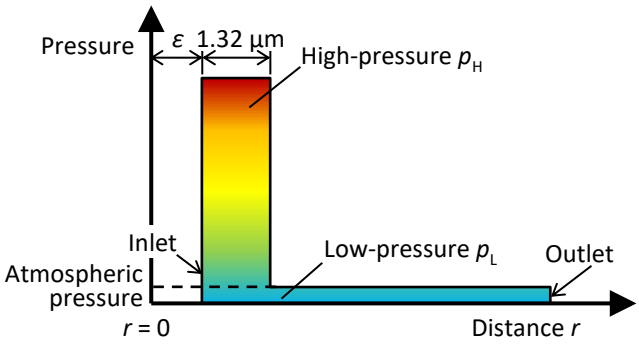


**Fig. 2.** Computational model

For the boundary conditions of calculating the 1-D model, density gradient, pressure gradient and velocity are fixed to be 0 at the inlet as the fixed-end boundary, and velocity gradient, density and pressure are fixed to be 0 at the outlet as the free-end boundary. On the other hand, in the case of the 1-D spherical symmetric model, the gradients of velocity, density and pressure are fixed to be 0 at the inlet and outlet as the symmetric boundary and the free-end boundary, respectively.

In both models, the initial high-pressure part was positioned a distance of $\varepsilon$ from the center line ($r$ = 0) to avoid the singularity. Here, the $\varepsilon$ is fixed to be 1.253 μm. In addition, the time step $\Delta t$ is 0.01 ns and the step size of distance $\Delta r$ is 69.6 nm. Figure 3 shows computational mesh. From Figure 3, the number of mesh at the high-pressure part and the low-pressure part are 19 and 4273 (at $r$ = 300 μm), respectively.

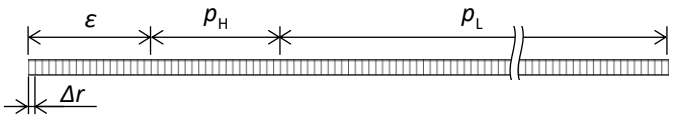


**Fig. 3.** Computational mesh

## 3. Computational Results without Effects of Bubble Behavior

### *3.1 Comparison of Propagation Characteristics of 1-D Model and 1-D Spherical Symmetric Model*

In this section, the peak pressure variation of shock waves with propagation as the propagation characteristics are compared between the 1-D model and the 1-D spherical symmetric model. Figure 4 shows the computed pressure histories at typical distances ($r$ = 1 μm, 100 μm, 200 μm, 300 μm) of the 1-D model and the 1-D spherical symmetric model, respectively. From Figure 4(a), during the propagation of the shock wave from 1 μm to 100 μm, the peak pressure in the case of the 1-D model decreased from 6.00 MPa to 2.77 MPa which is nearly 1/2. The peak pressure has been decreasing even after $r$ = 100 μm, the pressure was 2.32 MPa at $r$ = 300 μm. On the other hand, the pressure in the case of the 1-D spherical symmetric model decreased to 0.14 MPa at $r$ = 100 μm from 6.03 MPa at $r$ = 1 μm which is nearly 1/43 by the propagating (Figure 4(b)). From the comparison of the two models, the shock waves simulated in the 1-D spherical symmetric model were observed to attenuate earlier than in the 1-D model.

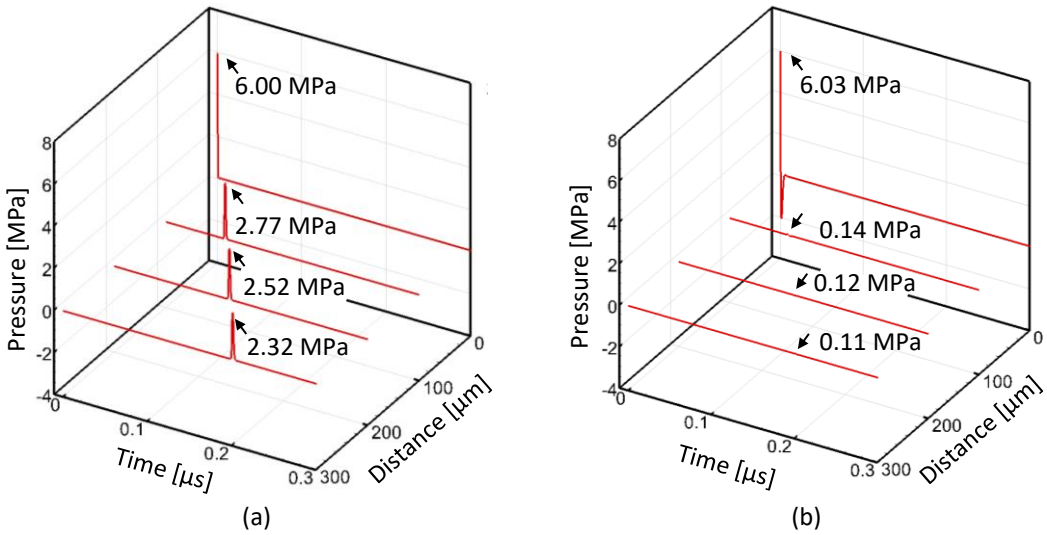


**Fig. 4.** Computed pressure history at each distance, (a) 1-D model, (b) 1-D spherical symmetric model

Next, the attenuation of pressure on the 1-D spherical symmetric model is examined in detail. Generally, the relationship between peak pressure and propagation distance on spherical shock waves can be approximated as follows:

$$P_{\max}(r) = \frac{\beta}{r^{\alpha}} \tag{9}$$

where $P_{\max}(r)$ is the peak pressure at each distance, $\alpha$ and $\beta$ are constants. Figure 5 shows the computed peak pressure at a distance from 1 μm to 50 μm on the 1-D spherical symmetric model. In this figure, the approximate curve is shown by dotted line. From Figure 5, $\alpha$ was determined to be 0.936 in this computation. Here $\alpha$ means gradient of attenuation on spherical shock waves, it was

reported that $\alpha$ is close to 1 in the case of laser-induced underwater shock waves from experiments by other researchers [8,10]. Therefore, it is confirmed the 1-D spherical symmetric model can simulate the laser-induced spherical shock waves, especially at the laser-focal area. In the following section, the result of the 1-D spherical symmetric model is compared with an experimental result.

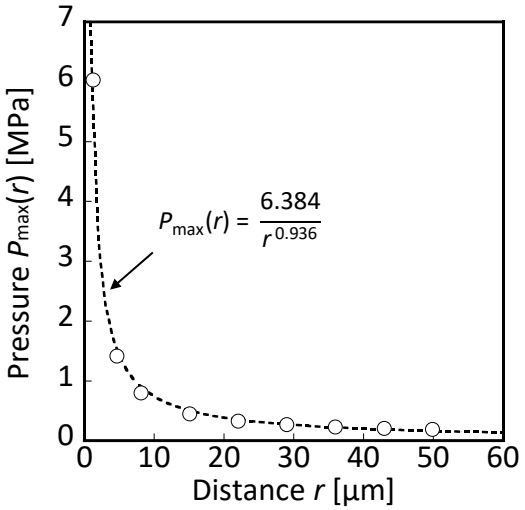


**Fig. 5.** Peak pressure of 1-D spherical symmetric model at $r$ = 1 μm to 50 μm

*3.2 Comparison of Waveform between 1-D Spherical Symmetric Model and Experiment*

Figure 6 shows the pressure history of the 1-D spherical symmetric model at $r$ = 300 μm and the experimental data at $r$ = 300 μm which was obtained from previous research [16]. For comparison, the pressure in both figures is shown as gauge pressure. From Figure 6(a), the peak pressure in the case of computation was nearly 0.01 MPa and the duration time of positive pressure was 5.62 ns. Here, duration time is the interval from the time when the pressure exceeds 0 MPa and the time when it returns 0 MPa. On the other hand, the peak pressure in the case of the experiment was 0.399 MPa and the duration time was 0.29 μs (290 ns) from Figure 6(b). From the comparison, it is confirmed that the both computed peak pressure and the duration time were much lower than the experimental result at the same distance.

In this connection, it is important to mention that the computational results do not include the effects of generated bubbles. However, the bubble generated at the laser-focal area had been observed in the experiments mentioned earlier [16]. From the disagreement, it is possible that the effect of bubbles changes the profile of the shock waves in the experiments. When bubbles and shock waves interfere with each other, micro jet is generated from the bubbles and the pressure of the shock wave is attenuated. In the previous research, the existence of small bubbles had not been investigated at the moment of laser focusing and shock wave generation. In the following section, the computation is conducted with the assumption that the bubbles are generated before the shock waves are generated.

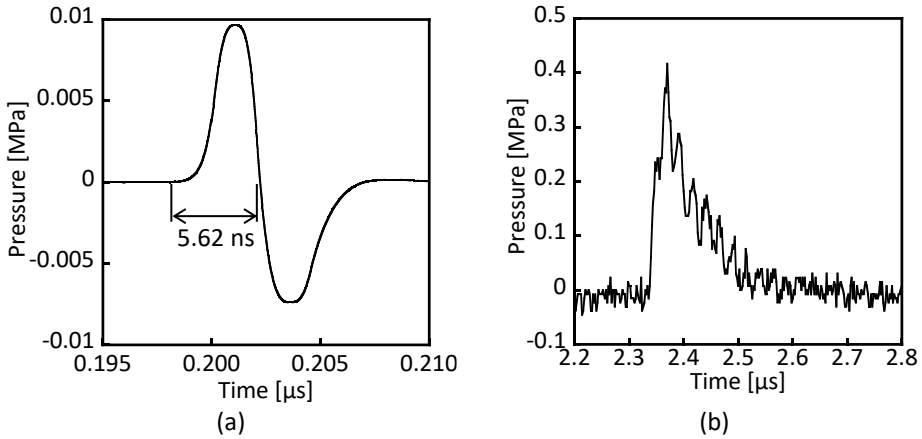


**Fig. 6.** Pressure history at $r$ = 300 μm, (a) 1-D spherical symmetric model, (b) Experiment

## 4. Computational Results Considering Effects of Bubble Behavior

### *4.1 Governing Equation for Behavior of Single Bubble*

The bubble vibrates in water by receiving waves such as shock waves and ultrasounds. In this computation, the following Rayleigh-Plesset equation is used as governing equation for the behavior of a single bubble in an incompressible fluid [20].

$$R\ddot{R} + \frac{3}{2}\dot{R}^2 = \frac{1}{\rho}\left\{p(R) - p_\infty(t) - \frac{4\mu\dot{R}}{R} - \frac{2\sigma}{R}\right\} \tag{10}$$

where $R$ is radius of bubble, $p(R)$ is internal pressure of bubble, $p_\infty(t)$ is pressure of surrounding liquid, $\rho$ is density of liquid, $\mu$ is viscosity of liquid, $\sigma$ is surface tension. When the bubble expands and contracts by fluctuation of $p_\infty(t)$, the internal pressure of the bubble is expressed following equation with the assumption that changing pressure of condensable gas is polytropic change.

$$p_g\left(\frac{4}{3}\pi R^3\right)^\gamma = p_{g0}\left(\frac{4}{3}\pi {R_0}^3\right)^\gamma \tag{11}$$

where $p_g$ is pressure of the condensable gas and $\gamma$ is polytropic exponent. The internal pressure of the bubble p is expressed as follows:

$$p = p_g + p_v = p_{g0}\left(\frac{R_0}{R}\right)^{3\gamma} + p_v = \left(p_{\infty 0} - p_v + \frac{2\sigma}{R_0}\right)\left(\frac{R_0}{R}\right)^{3\gamma} + p_v \tag{12}$$

where $p_v$ is vapor pressure. The following equation is obtained by substituting Eq. (12) for Eq. (10).

$$R\ddot{R} + \frac{3}{2}\dot{R}^2 = \frac{1}{\rho}\left\{\left(p_{\infty 0} - p_v + \frac{2\sigma}{R_0}\right)\left(\frac{R_0}{R}\right)^{3\gamma} + p_v - p_\infty(t) - \frac{4\mu\dot{R}}{R} - \frac{2\sigma}{R}\right\} \tag{13}$$

In this computation, changing radius and internal pressure of the bubble over time are computed by applying the pressure of the shock wave for $p_\infty(t)$ in Eq. (13). The numerical integration of Eq. (13) was conducted using Euler's method.

### *4.2 Calculation of Radius of Bubble by Rayleigh's Collapse Time*

Eq. (13) can be integrated when the bubble does not include the condensable gas with the assumptions that $p_v$ and $p_\infty$ are constant, $\mu$ and $\sigma$ are ignored. Rayleigh's collapse time which is the time for the radius of the bubble to change from minimum to maximum is expressed by double integration of Eq. (13) [20].

$$\tau = 0.915 R_0 \sqrt{\frac{\rho}{p_{\infty 0} - p_v}} \tag{14}$$

From Eq. (14), the period of bubble behavior is obtained. As the interaction between the shock wave and the bubble, here it is assumed the duration time of the shock wave is changed by the period of the bubble behavior. Based on the above assumption, the radius of the interfering bubble was calculated to be $R_0$ = 1.6 μm from Eq. (14) when the duration time was nearly 300 ns which was obtained from the previous experiment (Figure 6(b)) [16].

### *4.3 Computational Conditions for Interaction between Propagation of Shock Wave and Bubble Behavior*

The computation of the interaction is conducted as weak coupling through pressure. In the case of weak coupling, the computations are conducted by each other and given related parameters to each other. Regarding this coupling, shorter computation times and higher customizability are achieved at the cost of computational accuracy. To simplify the solving problem, the propagation of shock waves is computed as compressibility, and the behavior of the bubbles is computed as incompressibility.

As the computational conditions, the initial radius of the bubble is fixed to be $R_0$ = 1.6 μm and its position is fixed to be $r$ = 2.9 μm. If the initial internal pressure of the bubble is high, it will not vibrate by receiving the shock waves. Therefore, in this computation, to set the initial internal pressure as small as possible, $p_{\infty 0}$ is fixed to be 101.3 Pa which is 1/1000 of atmospheric pressure. In addition, $\rho$ is fixed to be 998.2 kg/m$^3$, $\mu$ is fixed to be 0.00854 Pa・s, $\sigma$ is fixed to be 71.69 mN/m, $\gamma$ is 1.4, $p_v$ is fixed to be 3.534 kPa and the time step $\Delta t$ is fixed to be 0.01 ns.

### *4.4 Computational Results of Interaction between Propagation of Shock Wave and Bubble Behavior*

Figure 7 shows computed pressure history of the 1-D spherical symmetric model at $r$ = 2.9 μm. Figure 8 shows changing radius ($R/R_0$) and internal pressure of the bubble over time at $r$ = 2.9 μm. Here, the initial high-pressure $p_H$ was fixed to be 6.0 MPa. From Figure 7, the peak pressure of the shock wave was 2.35 MPa, and the behavior of the bubble (Figure 8) was obtained by the bubble receiving this pressure. From Figure 8, the radius of the bubble changed and repeated to be expanded and contracted over time. In addition, the internal pressure also changed during the same vibration period to the changing radius, the maximum peak pressure was 0.492 MPa and the period was 299 ns.

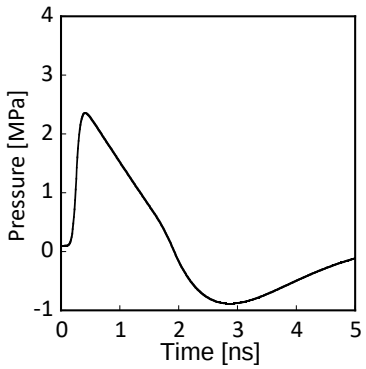


**Fig. 7.** Pressure history (pH = 6.0 MPa, r = 2.9 μm)

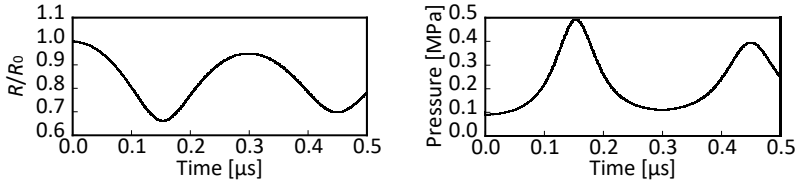


(a) (b)

**Fig. 8.** Behavior of bubble ($p_H$ = 6.0 MPa, $r$ = 2.9 μm)

Here, the interaction between the propagation of the shock wave and the bubble behavior is examined. Figure 9 shows the computed pressure wave obtained by the weak coupling between the pressure of the shock wave and the internal pressure at $r$ = 300 μm. From Figure 9, a small waveform was obtained around the time of 0.3 μs. The rise of the waveform was lenient and the peak pressure was 23.81 Pa (gauge pressure) which was near the atmospheric pressure. In addition, the duration time had extended from 5.62 ns to 50 ns, and this longer duration time is close to the experimental results which are influenced by bubbles. However, the peak pressure disagreed with the experimental result, the computed peak pressure became much lower than the experimental result. For this reason, it is possible that the set initial high-pressure and actual pressure at the laser-focal area are different. In our previous research, the pressure at the laser-focal area was estimated to be nearly 6.0 MPa [16]. However, it is not very accurate because of indirect measurement with the extrapolation method. In the following section, the initial computational conditions are reexamined and the results are compared.

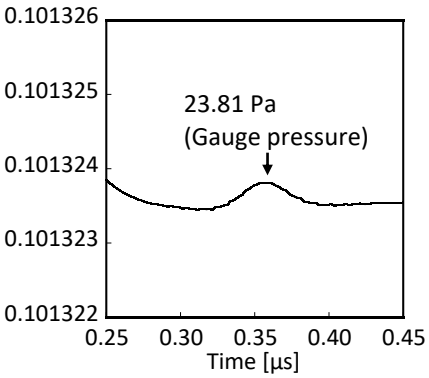


**Fig. 9.** Pressure wave ($p_H$ = 6.0 MPa, $r$ = 300 μm)

### *4.5 Effects of Initial Computational Conditions*

The actual pressure at the laser-focal area may be higher than 6.0 MPa which was estimated from the experiment. To investigate the effects of the initial high-pressure on the computed pressure wave, the $p_H$ was fixed to be 100 MPa. In this computation, 100 MPa is a limit pressure in Tait's state equation. Figure 10 shows the computed pressure history of the 1-D spherical symmetric model at $r$ = 2.9 μm in the case of $p_H$ = 100 MPa. Figure 11 shows the change in radius ($R/R_0$) and internal pressure of the bubble over time at $r$ = 2.9 μm in the case of $p_H$ = 100 MPa. Here, the computational conditions other than $p_H$ were fixed to be the same as the previous computation (section 4.4). From Figure 10, it is obtained the peak pressure of the shock wave was 36.42 MPa, which became higher than the peak pressure in the case of $p_H$ = 6.0 MPa (Figure 7). When the shock wave acted on the bubble, the bubble behavior was obtained in Figure 11. As the bubble behavior, the vibration period of the radius and the internal pressure were 293 ns, and the maximum peak pressure was 0.446 MPa. From these results, it is obtained that the vibration period was almost the same as the case of $p_H$ = 6.0 MPa. However, the pressure was slightly lower than it. The reason is considered the negative pressure became lower with increasing the initial high-pressure than in the case of $p_H$ = 6.0 MPa, the contraction of the bubble was stopped because of the action of tension.

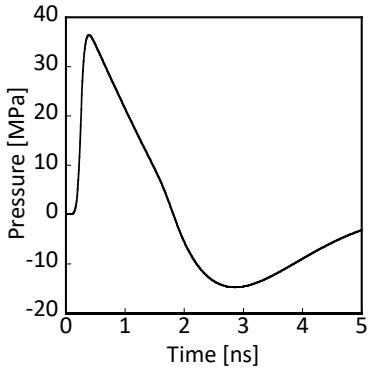


**Fig. 10.** Pressure history ($p_H$ = 100 MPa, $r$ = 2.9 μm)

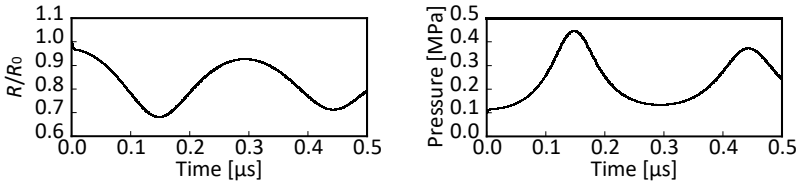


(a) (b)

**Fig. 11.** Behavior of bubble ($p_H$ = 100 MPa, $r$ = 2.9 μm)

Figure 12 shows computed pressure wave obtained by the weak coupling between the pressure of the shock wave and the internal pressure at $r$ = 300 μm in the case of $p_H$ = 100 MPa. From Figure 12, the peak pressure of the computed pressure wave was 24.52 Pa as gauge pressure, it was slightly higher than in the case of $p_H$ = 6.0 MPa. However, the peak pressure was the same as the atmospheric pressure even if $p_H$ was fixed to be 100 MPa.

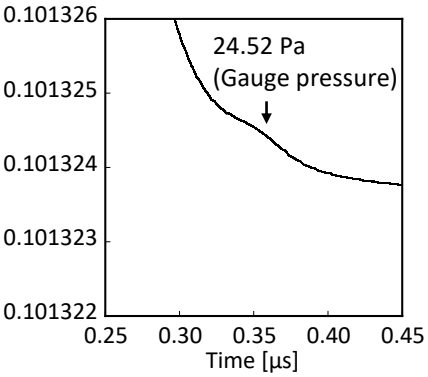


**Fig. 12.** Pressure wave ($p_H$ = 100 MPa, $r$ = 300 μm)

## 5. Discussion

Figure 13 shows the relationship between duration time and peak pressure of each computational condition and experimental result at $r$ = 300 μm. From Figure 13, the peak pressure in the case of the 1-D spherical symmetric model without the bubble behavior was relatively close to the experimental result. However, these duration times were quite different. On the other hand, the duration time of the computed wave in the case of $p_H$ = 6.0 MPa was relatively close to the experimental result. In addition, the duration time was longer than the 1-D spherical symmetric model when $p_H$ was fixed to be 100 MPa. From these results, the longer duration time can be obtained by considering the bubble behavior. However, these peak pressure were much lower than the experimental result. Even if the $p_H$ was fixed to be 100 MPa, the peak pressure was not changed much. The ratio between the experimental peak pressure and the computational peak pressure were 16758 times and 16727 times in the case of $P_H$ = 6.0 MPa and 100 MPa, respectively. It is possible to obtain the high peak pressure by setting $p_H$ to a much higher pressure. However, $p_H$ can be fixed until 100 MPa, the much higher pressure cannot be applied in this computational model. Therefore, the model used here cannot simulate the real phenomenon obtained from the experiments. In other words, to simulate the propagation of the shock wave exactly, it may be necessary to consider the effects of phenomena other than the bubble behavior. One example is the plasma that is known to generate when the fluid absorbs laser energy [14]. There is a possibility that other phenomena in generating process of the shock waves influence the propagation and the profile of the shock waves.

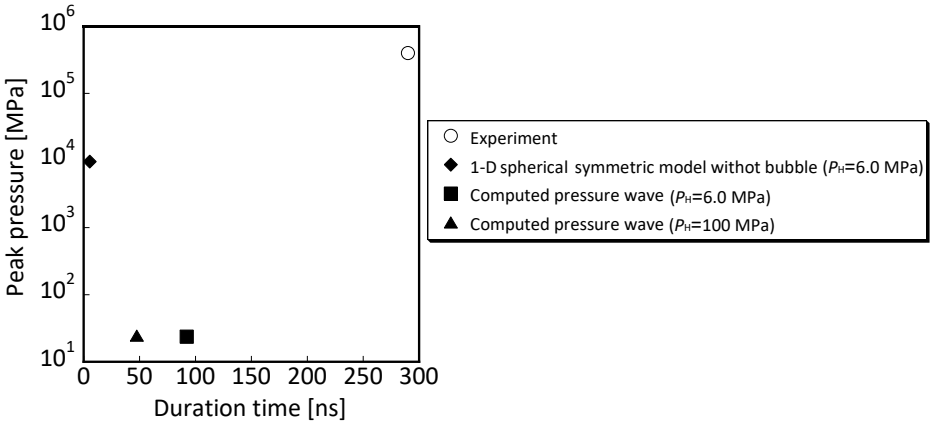


**Fig. 13.** Relationship between duration time and peak pressure

## 6. Conclusion

In this research, the numerical simulation is conducted to investigate the interactions between the propagation of the shock waves and the bubble behavior which are generated by focusing the femtosecond pulse laser. The following are concluded:

(i) From the comparison of the two computational models without the effects of the bubble behavior, the attenuation of the shock waves simulated in the 1-D spherical symmetric model was much earlier than in the case of the 1-D model.

(ii) The slope of the approximate curve related to the peak pressure and propagating distance was confirmed to be nearly 1, and the attenuation trend of the computed shock wave by the 1-D spherical symmetric model was roughly in agreement with the previous experiment. However, the computed peak pressure was not in agreement with the pressure obtained from the previous experiment.

(iii) From the computation by the 1-D spherical symmetric model with the bubble behavior, the internal pressure and vibration period of the bubble were obtained to be about 0.5 MPa and about 300 ns at the laser-focal area. However, the peak pressure of the computed wave became about 24 Pa as gauge pressure at the propagating distance of 300 μm.

(iv) To confirm the effects of the initial high-pressure, the pressure was fixed to be the maximum which was determined by Tait's state equation. Even in this condition, the peak pressure of the computed wave was almost the same as the atmospheric pressure. Therefore, it is suggested that there is a possibility that considering phenomena other than the bubble behavior is needed for the numerical simulation to compute the propagation of the shock waves exactly.

**Acknowledgment**
This work was supported by Grant-in-Aid for Scientific Research (B) 21H01252 and Grant-in-Aid for JSPS Fellows 23KJ1752.

## References

[1] Janardhanraj, S., and G. Jagadeesh. "Development of a novel miniature detonation-driven shock tube assembly that uses in situ generated oxyhydrogen mixture." *Review of Scientific Instruments* 87, no. 8 (2016). https://doi.org/10.1063/1.4960961

[2] Sundaram, Susinder, Karthi Sellamuthu, Krishnaveni Nagavelu, Harikumar R. Suma, Arpan Das, Raghu Narayan, Dipshikha Chakravortty, Jagadeesh Gopalan, and Sandeep M. Eswarappa. "Stimulation of angiogenesis using single-pulse low-pressure shock wave treatment." *Journal of Molecular Medicine* 96 (2018): 1177-1187. https://doi.org/10.1007/s00109-018-1690-1

[3] Takahashi, Toru, Keiichi Nakagawa, Shigeru Tada, and Akira Tsukamoto. "Low-energy shock waves evoke intracellular Ca2+ increases independently of sonoporation." *Scientific Reports* 9, no. 1 (2019): 3218. https://doi.org/10.1038/s41598-019-39806-x

[4] Tamagawa, Masaaki, Ichiro Yamanoi, and Atsushi Matsumoto. "Fundamental investigation for developing drug delivery systems and bioprocess with shock waves and bubbles (numerical analysis of deformation of cell model and observation of bubble behavior near the cell-membrane model)." *JSME International Journal Series C Mechanical Systems, Machine Elements and Manufacturing* 44, no. 4 (2001): 1031-1040. https://doi.org/10.1299/jsmec.44.1031

[5] Yamanoi, Ichiro, and Masaaki Tamagawa. "Deformation analysis of bubble near curved elastic wall for developing shock wave DDS." *JSME International Journal Series B Fluids and Thermal Engineering* 49, no. 3 (2006): 755-760. https://doi.org/10.1299/jsmeb.49.755

[6] Norio, Sanada, Takayama Kozuyoshi, and Ikeuchi Jun. "An Experimental Study of the Behavior of Bubbles and Shock Waves Generated by Laser Focusing in Water: Series B: Fluid Engineering Heat Transfer Combustion, Power Thermophysical Properties." *Transactions of the Japan Society of Mechanical Engineers Series B* 53, no. 486 (1987): 317-325. https://doi.org/10.1299/kikaib.53.317

[7] Yasuda, Takashi, Noriyuki Takahashi, Masafumi Baba, Kazuyoku Tei, and Shigeru Yamaguchi. "An experimental study on micro-bubble generation by laser-induced breakdown in water." *The Review of Laser Engineering* 36, no. APLS (2008): 1273-1275. https://doi.org/10.2184/lsj.36.1273

[8] Tagawa, Yoshiyuki, Shota Yamamoto, Keisuke Hayasaka, and Masaharu Kameda. "On pressure impulse of a laser-induced underwater shock wave." *Journal of Fluid Mechanics* 808 (2016): 5-18. https://doi.org/10.1017/jfm.2016.644

[9] Vogel, A., and W. Lauterborn. "Acoustic transient generation by laser-produced cavitation bubbles near solid boundaries." *The Journal of the Acoustical Society of America* 84, no. 2 (1988): 719-731. https://doi.org/10.1121/1.396852

[10] Vogel, Alfred, S. Busch, and U. Parlitz. "Shock wave emission and cavitation bubble generation by picosecond and nanosecond optical breakdown in water." *The Journal of the Acoustical Society of America* 100, no. 1 (1996): 148-165. https://doi.org/10.1121/1.415878

[11] Hosokawa, Y., H. Takabayashi, S. Miura, C. Shukunami, Y. Hiraki, and Hiroshi Masuhara. "Nondestructive isolation of single cultured animal cells by femtosecond laser-induced shockwave." *Applied Physics A* 79 (2004): 795-798. https://doi.org/10.1007/s00339-004-2823-7

[12] Sakai, Jun, Daniel Roldán, Kosei Ueno, Hiroaki Misawa, Yoichiroh Hosokawa, Takanori Iino, Shigeyuki Wakitani, and Mutsumi Takagi. "Effect of the distance between adherent mesenchymal stem cell and the focus of irradiation of femtosecond laser on cell replication capacity." *Cytotechnology* 64 (2012): 323-329. https://doi.org/10.1007/s10616-012-9437-2

[13] Iino, Takanori, Po-Lin Li, Wen-Zhe Wang, Jia-Huei Deng, Yun-Chang Lu, Fu-Jen Kao, and Yoichiroh Hosokawa. "Contribution of stress wave and cavitation bubble in evaluation of cell-cell adhesion by femtosecond laser-induced impulse." *Applied Physics A* 117 (2014): 389-393. https://doi.org/10.1007/s00339-014-8498-9

[14] Noack, Joachim, and Alfred Vogel. "Laser-induced plasma formation in water at nanosecond to femtosecond time scales: calculation of thresholds, absorption coefficients, and energy density." *IEEE Journal of Quantum Electronics* 35, no. 8 (1999): 1156-1167. https://doi.org/10.1109/3.777215

[15] Yamamoto, Ayumu, and Masaaki Tamagawa. "Fundamental Investigation of Generating Femtosecond Laser-Induced Underwater Shockwave for Development of Regenerative Medical System (Effects of Generated Bubble by Focusing Laser on Generation of Shockwave)." *Proceedings of the Kyushu Branch of the Japan Society of Mechanical Engineers* A15 (2021). https://doi.org/10.1299/jsmekyushu.2021.74.A15

[16] Yamamoto, Ayumu, Rintaro Obana, Kazuki Kara, and Masaaki Tamagawa. "Fundamental Investigation of Effects for Neutrophils Chemotaxis by Underwater Shockwave Stimulation (Effects of Plane Shockwave Using Shock Tube and Femtosecond Laser-Induced Spherical Shockwave)." *Proceedings of the BioFrontier Conference* 2B13 (2020). https://doi.org/10.1299/jsmebiofro.2020.31.2B13

[17] Vogel, Alfred, J. Noack, G. Hüttman, and G. J. A. P. B. Paltauf. "Mechanisms of femtosecond laser nanosurgery of cells and tissues." *Applied Physics B* 81 (2005): 1015-1047. https://doi.org/10.1007/s00340-005-2036-6

[18] Roe, Philip L. "Characteristic-based schemes for the Euler equations." *Annual Review of Fluid Mechanics* 18, no. 1 (1986): 337-365. https://doi.org/10.1146/annurev.fl.18.010186.002005

[19] Harten, Ami. "High Resolution Schemes for Hyperbolic Conservation Laws." *Journal of Computational Physics* 49, no. 3 (1983): 357-393. https://doi.org/10.1016/0021-9991(83)90136-5

[20] Franc, Jean-Pierre. "The Rayleigh-Plesset equation: a simple and powerful tool to understand various aspects of cavitation." In *Fluid Dynamics of Cavitation and Cavitating Turbopumps*, pp. 1-41. Vienna: Springer Vienna, 2007. https://doi.org/10.1007/978-3-211-76669-9_1